Energy Conversion and Management 297 (2023) 117706

Contents lists available at ScienceDirect

Energy Conversion and Management

journal homepage: www.elsevier.com/locate/enconman

Combined energy supply and management of self-powered wireless sensors based on radioisotope thermoelectric generator for multiple scenarios

Chen Wang [a], Zhiheng Xu [a,b,*], Hongyu Wang [a], Ting Cai [a], Haijun Tao [c], Yuqiao Wang [d], Xiaobin Tang [a,b]

[a] Department of Nuclear Science and Technology, Nanjing University of Aeronautics and Astronautics, Nanjing 210016, China
[b] Key Laboratory of Nuclear Technology Application and Radiation Protection in Astronautics, Ministry of Industry and Information Technology, Nanjing 211106, China
[c] College of Material Science and Technology, Nanjing University of Aeronautics and Astronautics, Nanjing 211100, China
[d] Research Center for Nano Photoelectrochemistry and Devices, School of Chemistry and Chemical Engineering, Southeast University, Nanjing 211189, China

ARTICLE INFO

Keywords:
Wireless Sensor Networks
Radioisotope Thermoelectric Generator
Energy Harvesting and Storage
Sensors

ABSTRACT

Nuclear battery technology, known for its ultra-long life, plays a unique role in a number of areas. The expanded applications of nuclear battery technology can reduce the weight and cost of wireless sensor networks as well as extend their lifecycle. In this work, a radioisotope thermoelectric generator (RTG) is proposed as a substitute for traditional batteries and then used for long-term generation of electrical energy. A direct current-direct current (DC-DC) converter is used to realize power management, and a super-capacitor is used to store the electrical energy generated by RTG. The changes in environmental temperature are detected using a sensor module. This work also explores the application of the combined system consisting of the above modules in different scenarios, such as confined space, unconfined space, and the deep-sea-polar region. In the deep-sea-polar region, the RTG can achieve a maximum power output of 4.32 mW. A DC-DC converter uses the LTC3108 to enable the optimization and stabilization of the electrical output of RTG in different working environments, the voltage generated by the RTG in millivolts is effectively and stably converted to a 3.7 V output, resulting in a significant increase in the maximum power output. Furthermore, the feasibility of using the RTG-charged super-capacitor to supply electricity for a wireless temperature sensor is demonstrated, providing a novel solution for long-term operations of wireless sensor network.

1. Introduction

Wireless sensor networks (WSNs) are playing an important role in a wide range of applications, including environmental monitoring [1], precision agriculture [2], water quality monitoring [3], and animal tracking [4], etc. At present, and well into the future, WSN is increasingly being deployed in various remote, harsh, and unmanned environments, which require sensor nodes to be functional for several months or even years. The utilization of chemical batteries as power sources for WSN cannot easily meet the requirements for long-term operation [5], the replacement of batteries can be cost prohibitive or even not feasible [6]. Waste chemical batteries will cause environmental pollution if they are not recycled properly; if some fuel cells are used, they will cause atmospheric pollution, global warming and other problems [7], threatening the survival of mankind. Thus, in order to reduce pollutant emissions and meet carbon neutrality targets [8], it is imperative to urgently identify a power source that can consistently, clean and reliably supply energy to WSN [9].

Energy harvesting is a technology for converting environmental energy into electricity. However, environmental energy sources, such as solar and wind energy, exhibit instability, making them less favorable for the continuous supply of energy to WSNs [10]. Radioisotope thermoelectric generator (RTG) [11] which operates based on the Seebeck effect [12–14], converts decay heat energy [15] from an isotopic heat source into electrical energy [16], exhibiting a long service life [17], high stability [18], and the lack of noise [19]. Despite these advantages, the electrical performance generated by the RTGs must be further improved for sensor nodes. Table 1 shows the energy consumption of some widely used sensor nodes. Some current research has focused on the miniaturization of RTG. For example, Yuan et al. [20] achieved the efficient, large-scale integration of modular single-layer devices by series–parallel stacking and reported that 900 pairs of thermoelectric (TE) legs can provide up to 13.2 V output. Liu et al. [21] synthesized two

* Corresponding author at: Department of Nuclear Science and Technology, Nanjing University of Aeronautics and Astronautics, Nanjing 211106, China.
E-mail address: xuzhiheng@nuaa.edu.cn (Z. Xu).

https://doi.org/10.1016/j.enconman.2023.117706
Received 19 August 2023; Received in revised form 19 September 2023; Accepted 24 September 2023

Nomenclature

V	output voltage of RTG, V
V_{oc}	the open-circuit voltage of the RTG, V
I	the output current of the RTG, A
I_{sc}	the short-circuit voltage of the RTG, A
P_{out}	the output power of the RTG, W
P_{max}	the maximum output power of the RTG, W
ΔT	the temperature difference of both sides of thermoelectric devices, K
T_h	hot side temperature, K
T_c	cold side temperature, K
L	length of thermoelectric leg, mm
S	cross-sectional area of thermoelectric leg, mm^2
R_{in}	the internal resistance in the RTG, Ω
R_L	the external load resistance in the RTG, Ω
η	conversion efficiency
ZT	thermoelectric merit of the thermoelectric materials
α	Seebeck coefficient, V/K
σ	electrical conductivity, S/m
ρ	resistivity, Ω·m
κ	thermal conductivity, W/(m·K)
N	number of thermoelectric pairs

Abbreviation

WSNs	wireless sensor networks
EH	energy harvesting
RTG	radioisotope thermoelectric generator
DC	direct current
V-I	voltage-current
P-I	power-current

Table 1
Energy consumption of sensor nodes [22].

Status	IRIS	MicaZ	IMote2	SunSpot	Waspmote	WiSMote
Sleep	8 μA	15 μA	390 μA	33 μA	55 μA	12 μA
Processing	8 mA	8 mA	31–53 mA	104 mA	15 mA	2.2 mA
Receive	16 mA	19.7 mA	44 mA	40 mA	30 mA	18.5 mA
Transmit	15 mA	17.4 mA	44 mA	40 mA	30 mA	18.5 mA
Supply	2.7–3.3 V	2.7 V	3.2 V	4.5–5.5 V	3.3–4.2 V	2.2–3.6 V

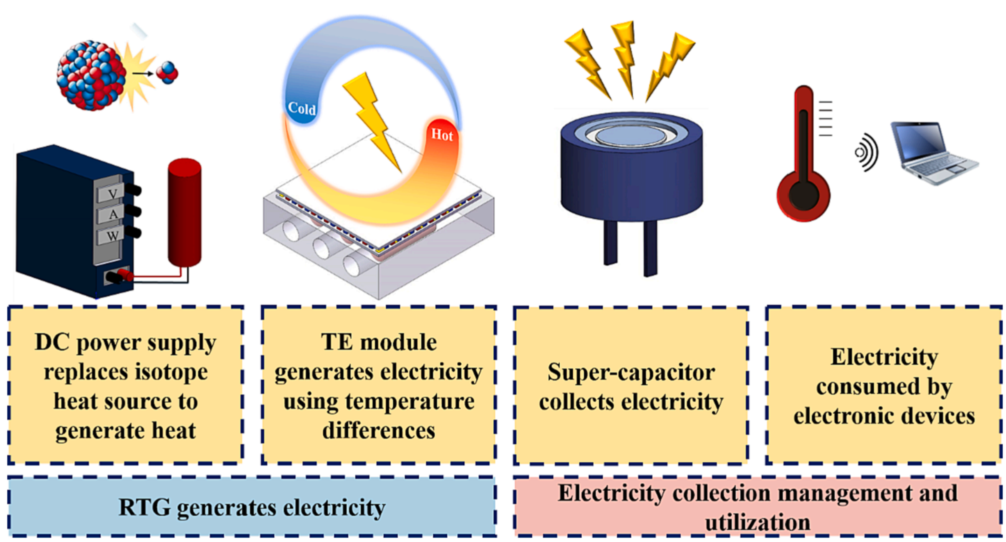

Fig. 1. The overall experimental testing device architecture of long-term system using the radioisotope thermoelectric generator (RTG).

small aerospace RTGs, and the fan–shaped and annular small–scale RTGs obtained V_{oc} of 1.17 and 1.56 V as well as P_{max} of 1.9 and 3.93 mW at 398.15 K, respectively. Although numerous studies have been conducted to optimize the output performance of TE modules, there are still many difficulties in providing direct power to a wireless sensor with a small number of TE modules.

Another approach is to use a direct current-direct current (DC-DC) converter for boosting the voltage. For example, Liu et al. [23] used a DC-DC converter to drive an electrocardiogram module in real time without the assistance of an additional power supply. Lü et al. [24] fabricated a wearable temperature sensor using the TE module and DC-DC converter. The abovementioned studies demonstrate that the DC-DC converter can effectively improve the power supply capability of the RTG.

According to the above literature review, it can be found that RTG has long life, cleanliness and other advantages over other batteries. Therefore, this paper proposes the use of RTG as a power source for WSN. Since there are few application cases of RTG, three equivalent working environments were set up, namely: the confined space, the unconfined space and the deep-sea-polar region, to explore the output performance of RTG in different working environments; meanwhile, in order to avoid the burden of volume, we only use one TE module to collect the heat generated by the equivalent heat source, which ensures the small size of the power supply and the adaptability to commercial sensor nodes. For better collection and management of the electricity generated by the RTG, a DC-DC converter was used to stably convert the

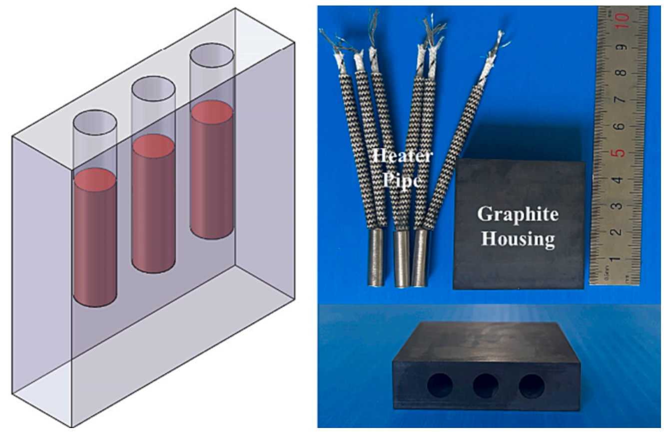

Fig. 2. Equivalent heat source structure schematic and physical diagram.

Table 2
Parameters of the components included in the equivalent heat source.

Component	Graphite Housing	Heater Pipe
Parameter	Length: 45 mm Width: 45 mm Thickness: 12 mm Internal hole diameter: 6 mm Internal hole height: 30 mm	Diameter: 6 mm Height: 20 mm Working limit: 24 V / 50 W

Table 3
Parameters of the TE module.

TE Module	Properties
Overall size/ mm × mm × mm	40 × 40 × 3.2
Number of component leg pairs	127
Operating temperature range/ K	273.15 ~ 523.15
N-type TE Material	Bi_2Te_3
P-type TE Material	Sb_2Te_3

output of the RTG. The converted electricity was stored in a super-capacitor and then used to power the sensor device. Finally, through the use of a power management switch (PMS) to interconnect the aforementioned components, a self-powered wireless sensor system has been successfully established, cycles autonomously without human intervention. For getting a more realistic picture of RTG in long-life working WSN, the operational runtime of two commonly used isotopic heat sources was calculated based on power density, thus serving as a reference working time for WSN.

2. Materials and methods

As depicted in Fig. 1, two pivotal factors ensure the long-term operation of the wireless Sensor Network (WSN) system: (a) the constant generation of electrical energy by the radioisotope thermoelectric generator (RTG) and (b) the subsequent collection of the generated electricity stored using a super-capacitor, thus enabling the accumulation of sufficient power to sustain the operation of the sensors.

2.1. Energy generation, conversion, and storage modules

To replace the isotopic heat source, a combination of a heater pipe and a graphite housing was utilized in our experiments, as shown in Fig. 2. A direct current (DC) power supply was used to provide current to the heater pipe in the equivalent heat source. The heater pipe converted electrical energy to resistance heat, while the design of an equivalent heat source took into account the volume size of the thermoelectric (TE) module. The three heater pipes were evenly placed in a series inserted into the graphite shell's holes. The corresponding geometrical parameters are shown in Table 2.

Commercial Bi_2Te_3 TE modules were chosen as the heat harvesting and electrical energy conversion component in the system. Table 3 presents the parameters of the TE module.

The direct current-direct current (DC-DC) converter model LTC3108 was selected for boosting, incorporating MOSFET switches, an external boost transformer, and small coupling capacitors to create a resonant boost oscillator for exceptional conversion performance. A super-capacitor (5.5 V 0.1F) was used as the energy storage device for effective energy harvesting and management.

2.2. Performance characterization

The TE module is mainly based on the Seebeck effect [25], which generates electromotive force when a temperature difference arises between the two ends of a semiconductor thermoelectric material [26]. The internal relationship between the electrical output of thermoelectric devices (e.g., open circuit voltage V_{oc} and output power P_{out}) and the material parameters of thermoelectric materials can be established when the temperature is stable. The specific calculation formula is as follows:

$$V_{oc} = \alpha\cdot(T_h - T_c)\cdot N \tag{1}$$

where α is the difference between the P-type material coefficient (positive) and the N-type material coefficient (negative); T_h and T_c denote the hot-end and cold-end temperatures of the TE module, respectively; and N denotes the number of thermocouples.

The internal resistance R_{in} of TE module is calculated as follows:

$$R_{in} = N\cdot(\rho_P + \rho_N)\cdot L/S \tag{2}$$

When the output end of TE module is connected to the load R_L to form a circuit, the current I flowing through the circuit can be expressed as:

$$I = \frac{\alpha\cdot(T_h - T_c)\cdot N}{R_{in} + R_L} \tag{3}$$

The output power P_{out} can be calculated as:

$$P_{out} = \frac{\alpha^2\cdot(T_h - T_c)^2\cdot N^2}{R_{in} + R_L} \tag{4}$$

Only when $R_{in} = R_L$ can the maximum output power P_{max} be obtained using the following equation:

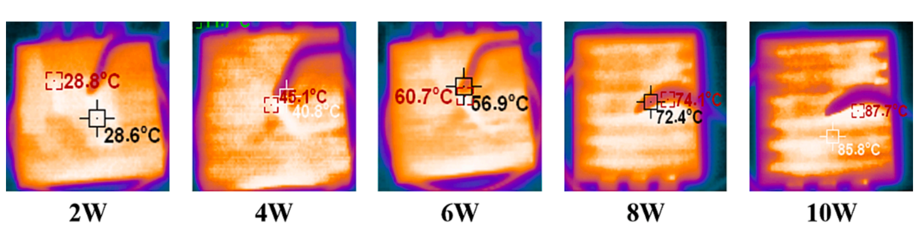

Fig. 3. Test results of the infrared thermometer for the surface temperature of the equivalent heat source: the thermal power levels are 2, 4, 6, 8, and 10 W.

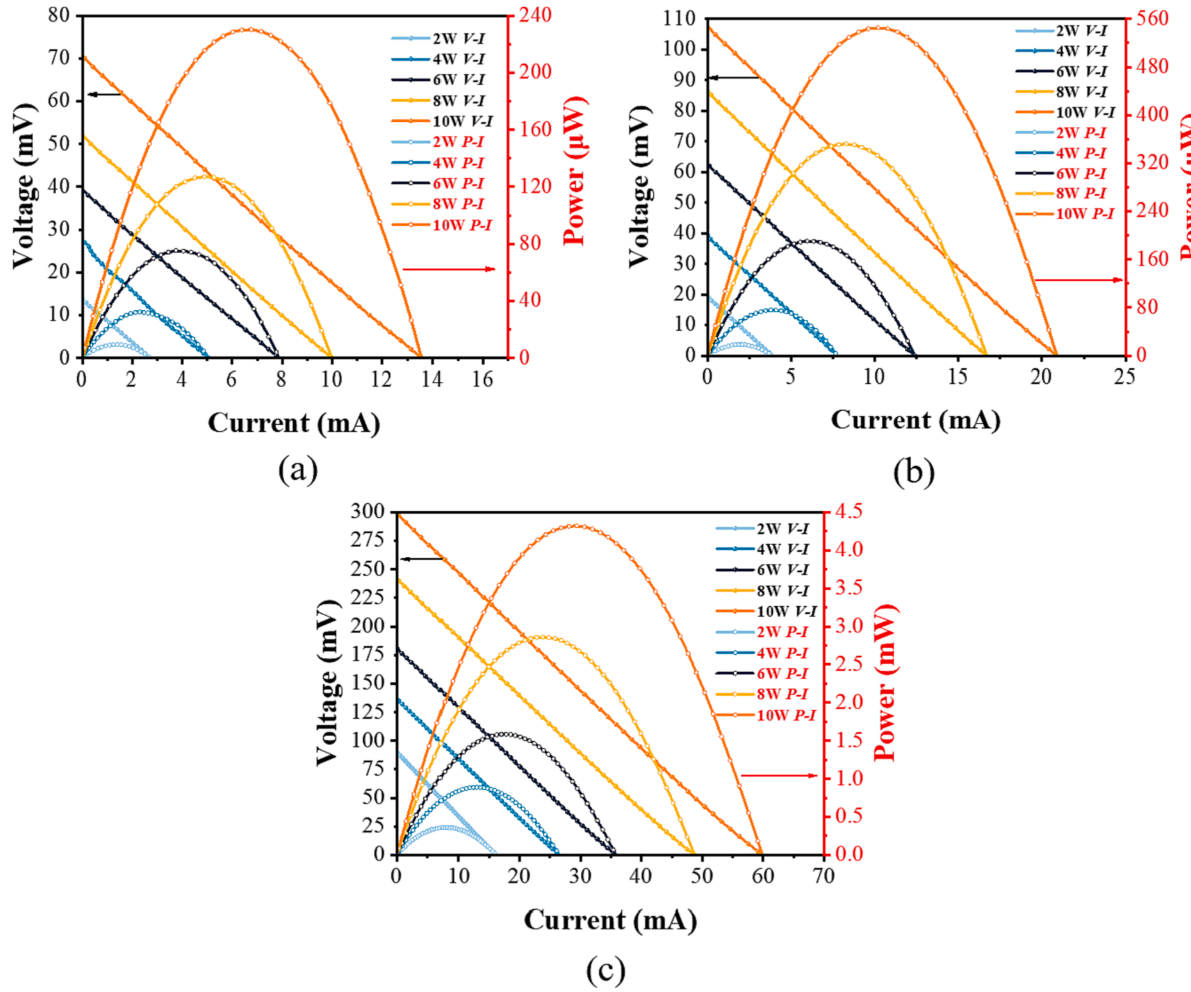

Fig. 4. *V-I/P-I* curves of the RTG in different working environments: (a) confined space, (b) unconfined space, and (c) deep-sea-polar.

$$P_{max} = \frac{\alpha^2 \cdot (T_h - T_c)^2 \cdot N^2}{4R_{in}} \tag{5}$$

3. Results and discussion

3.1. Equivalent analysis and performance study of heat sources

To simulate the decay process of the equivalent radioisotope, we continuously adjusted the thermal power to change the surface temperature of the equivalent heat source. Then, verification was conducted through the use of a thermocouple temperature sensor for supplementary testing purposes. Through correlation with the results of the thermocouple temperature sensor, the infrared thermometer can obtain accurate data. The thermal images are depicted in Fig. 3. As the heat spreads outwards, the temperature of the equivalent heat source surface gradually decreases, while the surface temperature of the heat source steadily increases with the increase of thermal power. Through the adjustment of thermal power applied to the equivalent heat source, a precise temperature range of 301.95–360.85 K can be achieved on the surface.

3.2. Electrical output performance of the RTG in different working environments

The space occupied by the RTG directly influences the flexibility of its deployment for power supply tasks. Moreover, the increasing integration of electronic devices has raised the demand for higher battery output. Therefore, conducting research on maximizing the electrical output performance of the RTG in a suitable working environment holds significant importance. Three distinct working environments were set, namely, confined space, unconfined space, and deep-sea-polar region. The settings of these working environments primarily focus on optimizing the space utilization of the RTG in practical applications and on enhancing its electrical output capacity.

The first environment pertains to the implementation of an RTG within a confined space, the equipment working in this environment typically imposes stringent size constraints, whose design necessitates compact dimensions. This restricts the entire power source to only include an equivalent heat source and a TE module. The voltage generated in this case relies on the heat dissipation capacity of the TE module itself. Fig. 4 (a) shows the I-V/P-V curves of the RTG working in a confined space at a different thermal power. When the thermal power of equivalent heat source is 10 W, RTG obtains 70 mV V_{oc}, 13.57 mA I_{sc}, and 230.26 μW P_{max}.

When the system is used in unconfined spaces, such as crop irrigation monitoring, meteorological studies, and flood monitoring, the RTG can be designed to be unlimited in size, and heatsinks can be considered to improve output performance. Due to the higher thermal conductivity of the heatsink in comparison to air, the heat transfer at the cold end of the TE module is significantly improved. This results in an increase in the temperature difference between the cold and hot ends, which in turn, leads to a substantial enhancement in electrical performance, as shown in Fig. 4 (b). When the thermal power of heat source is 10 W, the V_{oc} of RTG is 107 mV, which is about 1.4–1.5 times that of the RTG working in

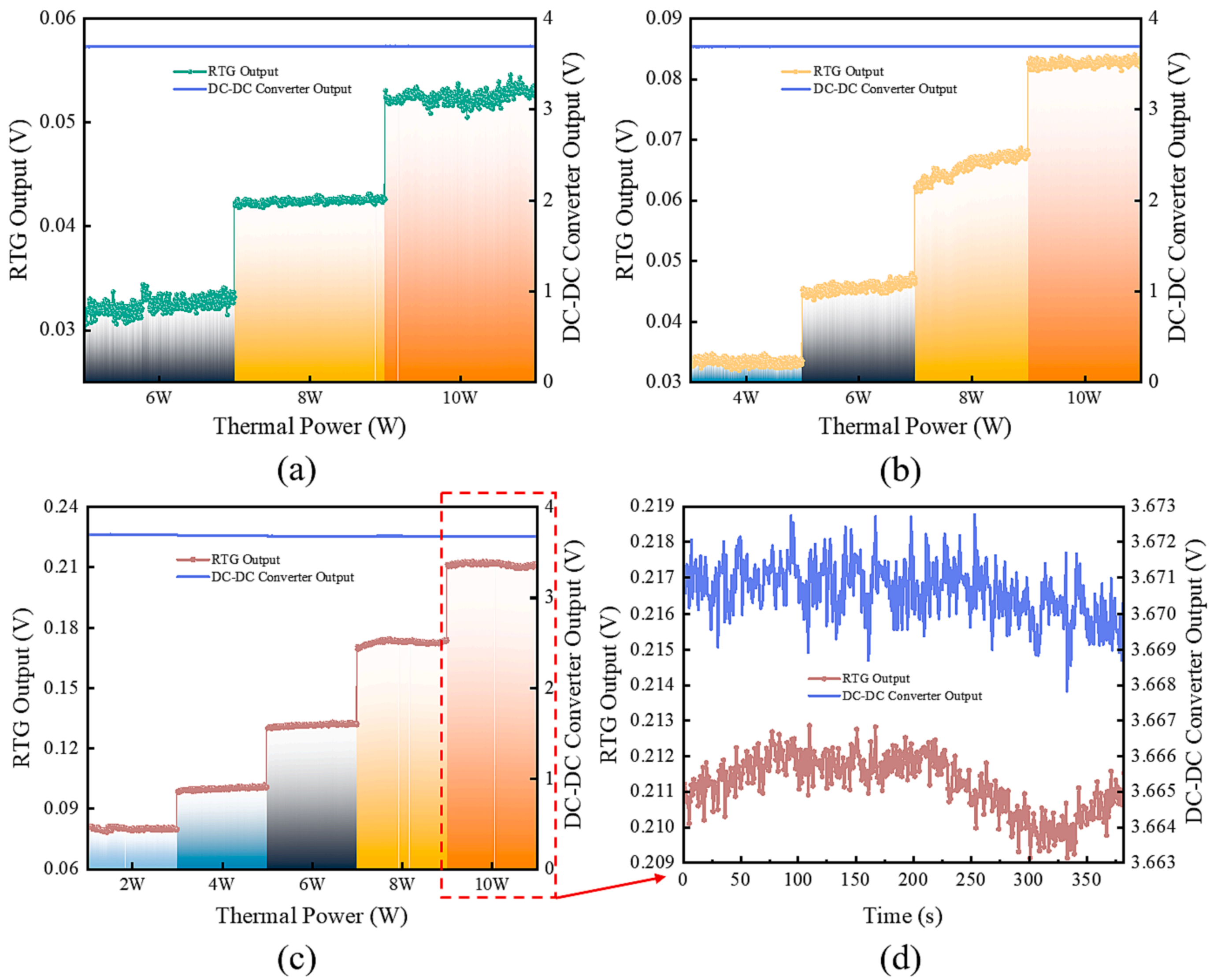

Fig. 5. The out voltages of the RTG and DC-DC converter: (a) In a confined space, (b) in an unconfined space, and (c) in the deep-sea-polar region, in which the columnar filling of different colors represents different thermal powers; (d) Close-up image of the RTG (@10 W) in deep-sea-polar.

confined space. In addition, I_{sc} is 21.10 mA and the P_{max} is 545.51 μW. Compared with the RTG working in confined space, the heatsink can significantly improve the output performance of TE module, and this enhancement is further amplified to a certain extent with an increase in the thermal power of heat source (from 2 to 10 W).

A water-cooling device was employed to connect to the cold side of the TE module to replace the deep-sea-polar working environment. The electrical performance is shown in Fig. 4 (c). As can be seen, when the thermal power is 10 W, the V_{oc} is 297 mV, the I_{sc} is 59.11 mA, and the P_{max} is 4.32 mW. Even in situations where the heat source power is low, RTG shows superior output performance when working in the deep-sea-polar region compared with its performance in confined and unconfined spaces. At the same time, RTG can improve output performance without the cost of volume and weight changes.

The V_{oc}, I_{sc}, and P_{max} of the RTG increase with increasing thermal power under different working environments, which is attribute to the temperature difference between the hot and cold ends of the TE module increasing with increasing thermal power of the heat source. Thus, it is imperative to consider the working environment before implementing the RTG. This is because a conducive working environment (low temperature or windy and rainy climate) has the potential to significantly enhance the performance of the RTG, which means that the utilization of excessively high temperature heat sources is unnecessary. Considering the prolonged operation of the RTG in standard environments, the temperature of the heat source gradually decreases, leading to a decline in its electrical output performance. In deep-sea polar environments, the RTG demonstrates excellent electrical output performance, even when the temperature of the heat source is low. This unique feature allows the RTG to reduce dependence on high temperature heat sources, thereby extending its working life.

3.3. The performance improvement effect of the DC-DC converter on the RTG

To test the improvement effect of the DC-DC converter, we collected data on the output end of both the RTG and DC-DC converter. Fig. 5 (a–c) depict the output voltages of the RTG and DC-DC converter. As can be seen, the RTG output voltage varies from 0.012 to 0.21 V due to the changes in heat source power and working scenes. In a confined space, the DC-DC converter can successfully convert the RTG output to 3.7 V when the thermal power ranges from 6 to 10 W. In an unconfined space, successful voltage conversion occurs at a heat source power ranging

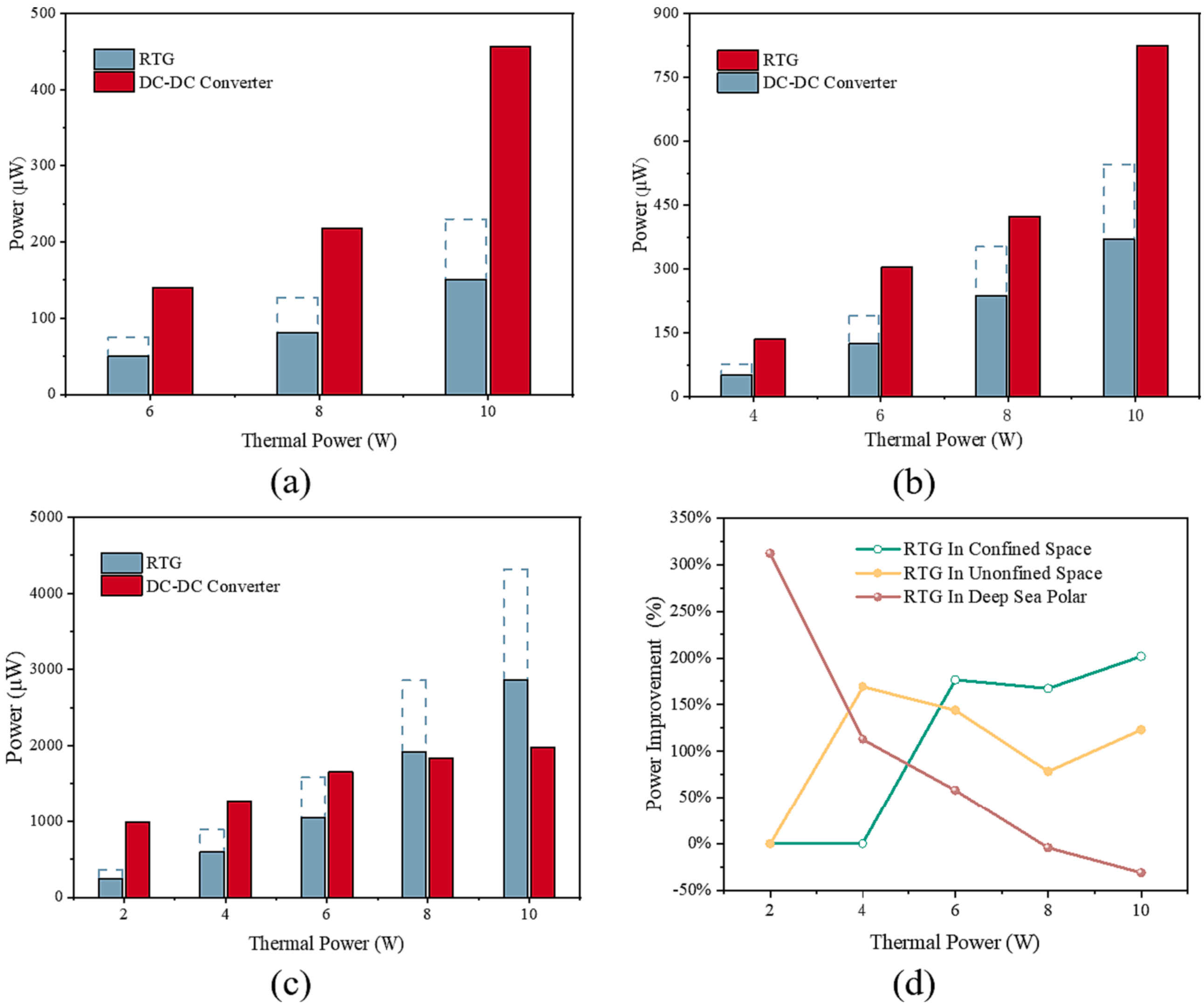

Fig. 6. The output power of the RTG and DC-DC converter in different working environments: (a) confined space, (b) unconfined space, (c) deep-sea-polar region, in which the dashed box represents the P_{max} of RTG; (d) The power improvement of DC-DC converter.

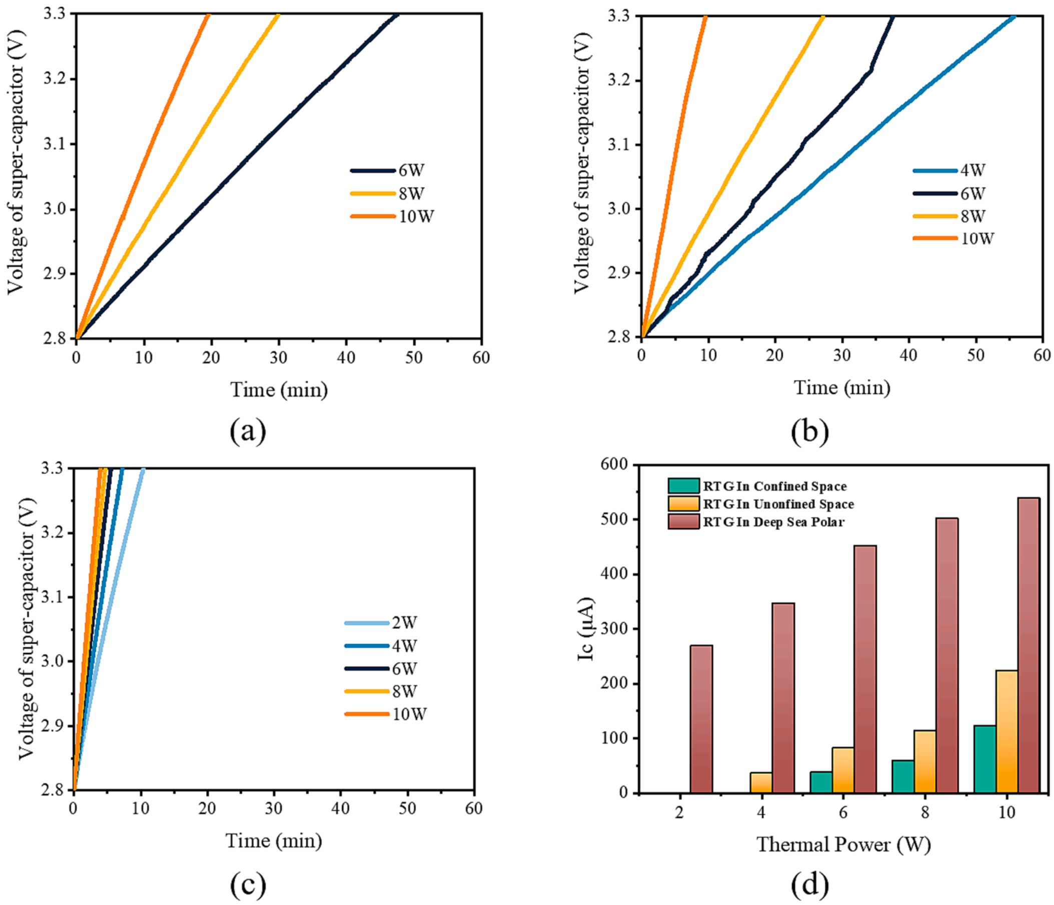

Fig. 7. Charging curves of the super-capacitor in different working environments: (a) confined space, (b) unconfined space, (c) deep-sea-polar, and (d) charging current I_c.

from 4 to 10 W. In the deep-sea-polar region, such conversion is achieved when the heat source power ranges from 2 to 10 W. Fig. 5 (d) provides close-up images of the RTG output and DC-DC converter in the deep-sea-polar region when the heat source's thermal power is 10 W. Notably, the output signal of the DC-DC converter remains stable even when the TE module output voltage fluctuates.

Moreover, the alterations in the output power of the RTG prior to and subsequent to the use of a DC-DC converter were further discussed. For an energy storage device, a higher charging power results in a shorter charging time to reach full capacity. After conversion through the DC-DC converter, a significant change can be observed in the output power of the RTG. As shown in Fig. 6, the influence of the DC-DC converter on the RTG output power is not always positive. When the V_{oc} range of the RTG is between 39.51 and 180.18 mV, the average output power after DC-DC conversion increases by a maximum of 311.91 % compared with the average output power of the RTG. However, when the V_{oc} of the RTG is more than 240.04 mV, the output power after conversion actually decreases, the lack of maximum power point tracking function prevents the adjustment of the chip's internal resistance and hampers the energy collector's ability to output maximum power. Based on the experimental situation, we can further explore how we can improve the electrical output of RTG in specific scenarios, such as changing the numbers of the P/N type thermoelectric leg, which is a means of altering the output voltage. At the same time, the RTG for deep-sea-polar regions has excellent output performance due to the unique natural cold source environment. Lower power heat sources or TE modules with fewer thermoelectric legs can be used in this scenario to mitigate the negative effect of using a DC-DC converter.

3.4. Energy management and power supply application performance evaluation

To collect and store the electric energy generated by the RTG, a super-capacitor (5.5 V 0.1F) was connected to the output end of the DC-DC converter. The experimental results are shown in Fig. 7.

Within the thermal power range where the DC-DC converter can be successfully started, the RTG can effectively accumulate electricity in the super-capacitor. As the power of the heat source increases and the working environment changes, the amount of electricity stored in the super-capacitor gradually increases. When the RTG operates within a confined space, the charging time for the capacitor to reach 2.8–3.3 V ranges from 19 to 47 min. In an unconfined space environment, the charging time varies from 9.5 to 55 min. However, in deep-sea-polar conditions, the charging time is significantly reduced to a range of 4–10 min. At the same time, by calculating the charging current I_c of the super-capacitor, it can also be noticed that the current generated by the RTG decreases after the conversion of the DC-DC converter. However, the overall trend is consistent with the I_{sc} of the TE module, as shown in Section 3.2.

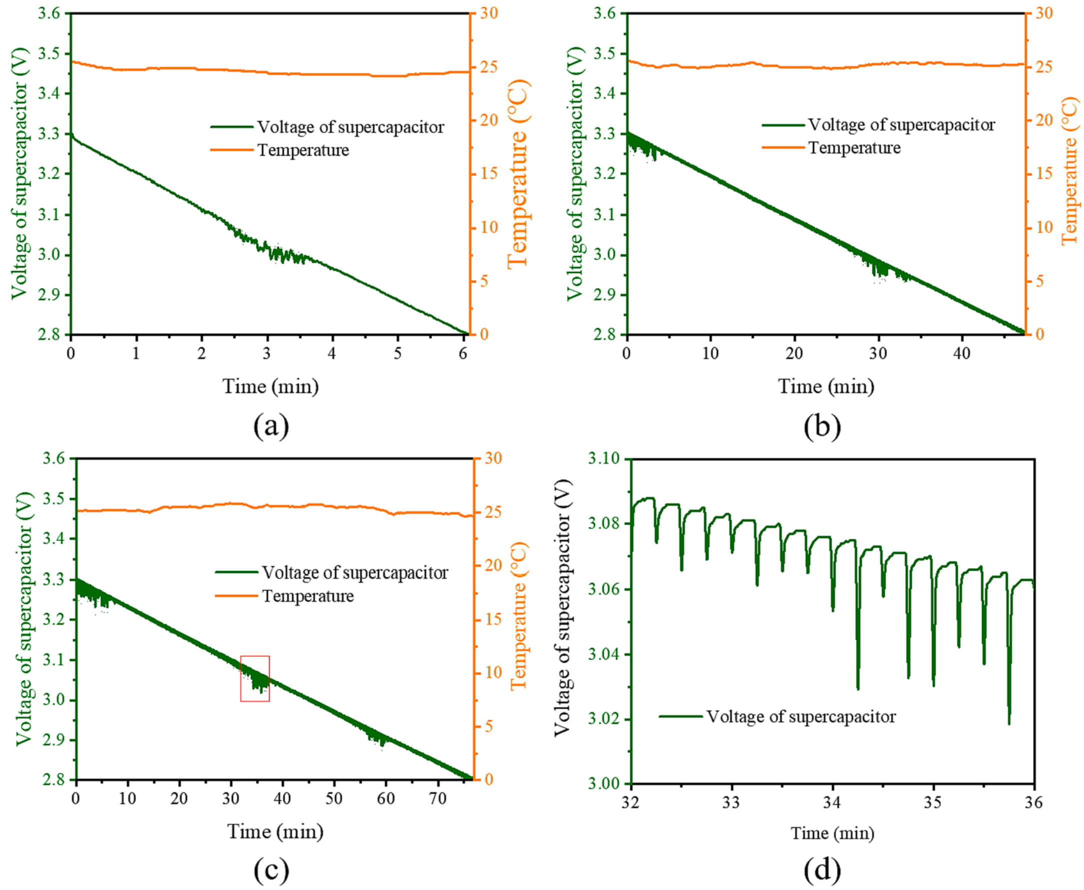

Fig. 8. Discharging curves of the super-capacitor (green) and different cycles of transmitting environmental temperature signal (orange): (a) 1 s, (b) 8 s, (c) 15 s, and (d) enlarged view of curve cluster.

Table 4
Radioisotope heat source material properties [31].

Parameters	$^{238}PuO_2$	$^{90}SrTiO_3$
Half-life of isotope ($T_{1/2}$, year)	87.7	28.9
Type of decay	α	β
Initial volumetric power density (W/cm^3)	5.52	4.54

To verify the signal wireless communication transmission, two ZigBee modules were used: one for sensing device to monitor the environmental temperature and the other for connecting to the computer as the data receiver. During the testing process, the signal transmission cycles of 1, 8, and 15 s were respectively modified.

Implementing longer time intervals can effectively mitigate power shortages. Therefore, by transmitting sensing signals at regular intervals of several hours or days, wireless sensors can maintain signal transmission for an extended duration, allowing them to wait for subsequent energy collection opportunities. Specifically, with a 1 s data cycle, the wireless sensor can operate continuously for 6 min, as shown in Fig. 8 (a), whereas a 15 s data cycle can lead to 76 min of uninterrupted operation, as shown in Fig. 8 (c). During the testing process, a noteworthy phenomenon was observed: after the sensor transmitted data once, the voltage of the super-capacitor initially declined and then rapidly increased, resulting in the formation of a "curve cluster," as depicted in Fig. 8 (b) and (c). Furthermore, Fig. 8 (d) provides an enlarged view of the clusters. This phenomenon, known as "voltage recovery," is caused by the charge redistribution in the super-capacitor electrodes [27–30]. These results indicate that super-capacitors can be used effectively to serve as an energy storage system, while simultaneously reducing the requirement for RTG output energy by extending the data cycle of the sensors.

3.5. Design and evaluation of the long-term working wireless sensor

The key to the RTG's longevity lies in the fact that the isotopic heat source in its components is capable of generating heat continuously—a process that is theoretically infinite. However, as the isotopes used in the heat source continue to decay, the amount of heat generated decreases, resulting in a gradual decline in the output performance of the RTG. To evaluate the performance of the RTG after it is put into operation in WSN, we conducted an analysis of the self-power attenuation of two types of isotope heat sources during long-term use based on their characteristics. The main characteristics of the heat source materials are shown in Table 4.

The results of the self-power attenuation are presented in Fig. 9 (a). The operating times of the equivalent heat source was calculated using the power density values and the half-life of two kinds isotope heat sources. The results are shown in Fig. 9 (b). As can be seen, within the thermal power range of 6–10 W, $^{238}PuO_2$ can sustain effective operation for decades. In practical usage, a power management switch (PMS) can be used to realize automatic discharge and charge of the super-capacitor.

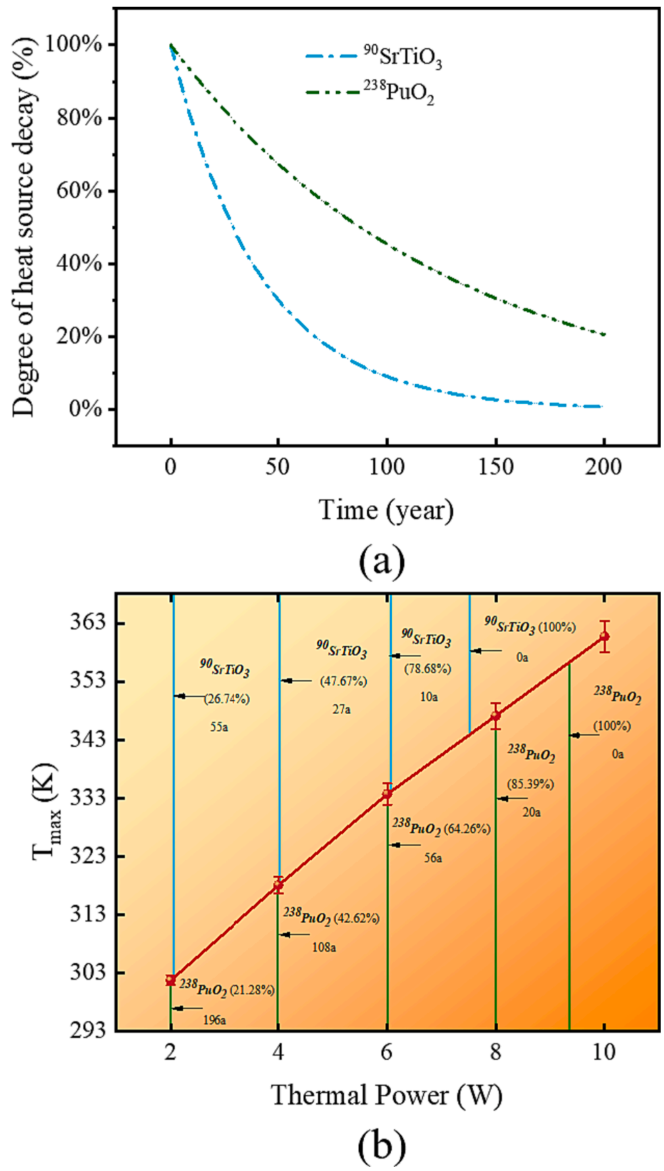

Fig. 9. (a) Calculation of the cumulative power attenuation of $^{238}PuO_2$ and $^{90}SrTiO_3$ over 200 years; (b) Equivalent evaluation of working time based on $^{238}PuO_2$ and $^{90}SrTiO_3$ isotope heat sources.

Based on the experiments presented in Section 3.4, a super-capacitor requires a certain charging time to power wireless sensors. This leads to waiting times during the long-term operation of the wireless sensor. The electrical energy generated by the RTG is accumulated and stored in the super-capacitor via Switch 1. When the super-capacitor's voltage remains within the range of the current maximum (V_{max}) and minimum (V_{min}) voltages, the Switch 2 is turned on and it can connections the super-capacitor power the sensor until the voltage level drops to V_{min}, at which point Switch 2 is turned off. The monitoring and recording results obtained using PMS are depicted in the Fig. 10. After turning on Switch 1, the super-capacitor takes 18.9 min to charge from 3 to 3.6 V. Once the voltage of the super-capacitor reaches V_{max}, the Switch 2 will be activated, and the stored energy in the super-capacitor is discharged to power the wireless sensor. If the voltage falls below V_{min}, the sensor temporarily ceases operation until the super-capacitor is recharged to 3.6 V, at which point the sensor is reactivated. The duration of this process is dependent on the charging characteristics described in Section 3.4.

4. Conclusion

A self-powered WSN system can be formed by connecting the RTG, DC-DC converter, and super-capacitor together using a PMS. The whole system outputs the power generated by the RTG and has no other electrical inputs. The output performance of RTG in three operating environments: confined space, unconfined space, and deep-sea polar region, shows that the size design of RTGs as well as the application requirements of electrical output performance parameters can be considered according to the specific operating environments. In deep-sea polar, RTG without heatsink can achieve the output performance that the V_{oc} is 297 mV, the I_{sc} is 59.11 mA, and the P_{max} is 4.32 mW. By using a DC-DC converter, the output capacity of the RTG can be effectively increased; as the output voltage is increased by the converter, as well as the output power. However, this change is not always positive, which is highly dependent on the output voltage of the RTG. Harvesting electrical energy generated by the RTG, the super-capacitor can be charged from 2.8 to 3.3 V in a few to 10 min, depending on the power of the heat source and the working environment. This charge can power the sensor for up to dozens of minutes, and the system can maintain consistency over multiple cycles.

This work also has great potential for energy harvesting and reuse. The TE module can effectively capture and utilize other waste heat energy sources such as waste heat from machinery/vehicles in industrial production, geothermal/solar energy in the daily environment, and heat generated by the human body, which can be converted into electricity to power other electronic devices in various fields. This study presents new insights into the applications of RTG and provides a valuable reference for future deep space exploration missions.

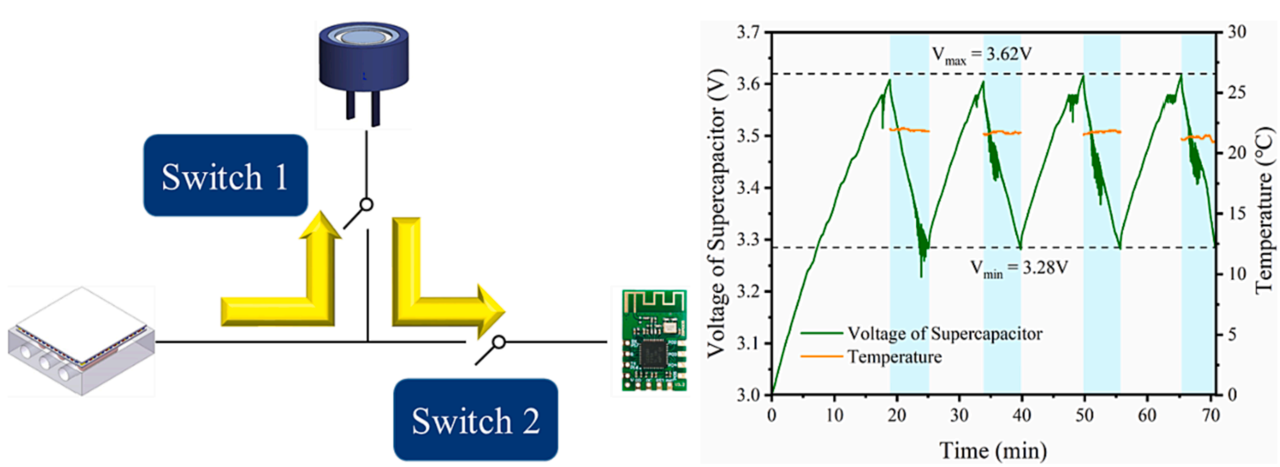

Fig. 10. Monitoring of the super-capacitor voltage under wireless sensor with transmitting signal cycles of 1 s when the RTG (@10 W) is in an unconfined space.

CRediT authorship contribution statement

Chen Wang: Conceptualization, Methodology, Writing – original draft. **Zhiheng Xu:** Conceptualization, Writing – review & editing. **Hongyu Wang:** Validation, Writing – review & editing. **Ting Cai:** Formal analysis, Writing – review & editing. **Haijun Tao:** Visualization, Writing – review & editing. **Yuqiao Wang:** Methodology, Writing – review & editing. **Xiaobin Tang:** Methodology, Writing – review & editing.

Declaration of Competing Interest

The authors declare that they have no known competing financial interests or personal relationships that could have appeared to influence the work reported in this paper.

Data availability

Data will be made available on request.

Acknowledgment

This work was supported in part by the Shanghai Aerospace Science and Technology Innovation Project (Grant No. SAST2020-097), the Natural Science Foundation of Jiangsu Province (Grant No. BK20201288), the Fundamental Research Funds for the Central Universities (Grant No. NT2023013), and Jiangsu Funding Program for Excellent Postdoctoral Talent (Grant No. 2022ZB235).

References

[1] Ali A, Khelil A, Shaikh FK, Suri N. Efficient predictive monitoring of wireless sensor networks. IJAACS 2012;5:233. https://doi.org/10.1504/IJAACS.2012.047657.
[2] Fang LG, Liu ZB, Li HL, Gu CD, Dai ML. Application of wireless sensor network for M2M in precision fruits. AMR 2011;267:482–7. https://doi.org/10.4028/www.scientific.net/AMR.267.482.
[3] Kageyama T, Miura M, Maeda A, Mori A, Lee S-S-A. wireless sensor network platform for water quality monitoring. IEEE SENSORS. Orlando, FL, USA: IEEE 2016;2016:1–3. https://doi.org/10.1109/ICSENS.2016.7808887.
[4] Duda N, Nowak T, Hartmann M, Schadhauser M, Cassens B, Wägemann P, et al. BATS: Adaptive ultra low power sensor network for animal tracking. Sensors 2018;18:3343. https://doi.org/10.3390/s18103343.
[5] Ijemaru GK, Ang KL-M, Seng JK. Wireless power transfer and energy harvesting in distributed sensor networks: Survey, opportunities, and challenges. 155014772110677 Int J Distrib Sens Netw 2022;18. https://doi.org/10.1177/15501477211067740.
[6] Teresa Penella M, Albesa J, Gasulla M. Powering wireless sensor nodes: Primary batteries versus energy harvesting. In: 2009 IEEE Intrumentation and Measurement Technology Conference. Singapore. Singapore: IEEE; 2009. p. 1625–30. https://doi.org/10.1109/IMTC.2009.5168715.
[7] Dai B, Qi H, Liu S, Zhong Z, Li H, Song M, et al. Environmental and economical analyses of transcritical CO2 heat pump combined with direct dedicated mechanical subcooling (DMS) for space heating in China. Energ Conver Manage 2019;198:111317. https://doi.org/10.1016/j.enconman.2019.01.119.
[8] Dai B, Wang Q, Liu S, Wang D, Yu L, Li X, et al. Novel configuration of dual-temperature condensation and dual-temperature evaporation high-temperature heat pump system: Carbon footprint, energy consumption, and financial assessment. Energ Conver Manage 2023;292:117360. https://doi.org/10.1016/j.enconman.2023.117360.
[9] Mazunga F, Nechibvute A. Ultra-low power techniques in energy harvesting wireless sensor networks: Recent advances and issues. Scientific African 2021;11:e00720. https://doi.org/10.1016/j.sciaf.2021.e00720.
[10] Grossi M. Energy harvesting strategies for wireless sensor networks and mobile devices: A review. Electronics 2021;10:661. https://doi.org/10.3390/electronics10060661.
[11] Xing Y, Liu R, Liao J, Wang C, Zhang Q, Song Q, et al. A device-to-material strategy guiding the "Double-High" thermoelectric module. Joule 2020;4:2475–83. https://doi.org/10.1016/j.joule.2020.08.009.
[12] Gürkan K, Karaman H, Ballikaya S. Optimization of high-performance flexible thermoelectric generator from material synthesis to simulation and device application. Energ Conver Manage 2023;291:117335. https://doi.org/10.1016/j.enconman.2023.117335.
[13] Rösch AG, Franke L, Mallick MdM, Lemmer U. Optimizing printed thermoelectric generators with geometry and processibility limitations. Energ Conver Manage 2023;279:116776. https://doi.org/10.1016/j.enconman.2023.116776.
[14] Zhu P, Luo X, Lin X, Qiu Z, Chen R, Wang X, et al. A self-healable, recyclable, and flexible thermoelectric device for wearable energy harvesting and personal thermal management. Energ Conver Manage 2023;285:117017. https://doi.org/10.1016/j.enconman.2023.117017.
[15] Wang G, Hu R, Wei H, Zhang H, Yang Y, Xiong X, et al. The effect of temperature changes on electrical performance of the betavoltaic cell. Appl Radiat Isot 2010;68:2214–7. https://doi.org/10.1016/j.apradiso.2010.06.011.
[16] Prelas M, Boraas M, De La Torre AF, Seelig J-D, Tchakoua Tchouaso M, Wisniewski D. Nuclear Batteries and Radioisotopes 2016;vol. 56. https://doi.org/10.1007/978-3-319-41724-0.
[17] Gusev VV, Pustovalov AA, Rybkin NN, Anatychuk LI, Demchuk BN, Ludchak IY. Milliwatt-power radioisotope thermoelectric generator (RTG) based on plutonium-238. Journal of Elec Materi 2011;40:807–11. https://doi.org/10.1007/s11664-011-1579-z.
[18] Liu K, Tang X, Liu Y, Xu Z, Yuan Z, Li J, et al. Preparation and optimization of miniaturized radioisotope thermoelectric generator based on concentric filament architecture. J Power Sources 2018;407:14–22. https://doi.org/10.1016/j.jpowsour.2018.10.052.
[19] Xu Z, Li J, Tang X, Liu Y, Jiang T, Yuan Z, et al. Electrodeposition preparation and optimization of fan-shaped miniaturized radioisotope thermoelectric generator. Energy 2020;194:116873. https://doi.org/10.1016/j.energy.2019.116873.
[20] Yuan Z, Tang X, Cabot A, Xu Z, Liu K, Wang H, et al. High-performance micro-radioisotope thermoelectric generator with large-scale integration of multilayer annular arrays through screen printing and stacking coupling. Energy Tech 2021;9:2001047. https://doi.org/10.1002/ente.202001047.
[21] Liu K, Tang X, Liu Y, Xu Z, Yuan Z, Ji D, et al. Experimental optimization of small–scale structure–adjustable radioisotope thermoelectric generators. Appl Energy 2020;280:115907. https://doi.org/10.1016/j.apenergy.2020.115907.
[22] Shaikh FK, Zeadally S. Energy harvesting in wireless sensor networks: A comprehensive review. Renew Sustain Energy Rev 2016;55:1041–54. https://doi.org/10.1016/j.rser.2015.11.010.
[23] Fan W, An Z, Liu F, Gao Z, Zhang M, Fu C, et al. High-performance stretchable thermoelectric generator for self-powered wearable electronics. Adv Sci 2023;10:2206397. https://doi.org/10.1002/advs.202206397.
[24] Shi Y, Lü X, Xiang Q, Li J, Shao X, Bao W. Stretchable thermoelectric generator for wearable power source and temperature detection applications. Energ Conver Manage 2022;253:115167. https://doi.org/10.1016/j.enconman.2021.115167.
[25] Markiewicz M, Dziurdzia P, Konieczny T, Skomorowski M, Kowalczyk L, Skotnicki T, et al. Software controlled low cost thermoelectric energy harvester for ultra-low power wireless sensor nodes. IEEE Access 2020;8:38920–30. https://doi.org/10.1109/ACCESS.2020.2975424.
[26] Karabetoglu S, Sisman A, Fatih Ozturk Z, Sahin T. Characterization of a thermoelectric generator at low temperatures. Energ Conver Manage 2012;62:47–50. https://doi.org/10.1016/j.enconman.2012.04.005.
[27] Subramanian S, Johny MA, Malamal Neelanchery M, Ansari S. Self-discharge and voltage recovery in graphene supercapacitors. IEEE Trans Power Electron 2018;33:10410–8. https://doi.org/10.1109/TPEL.2018.2810889.
[28] Torregrossa D, Bahramipanah M, Cherkaoui R, Paolone M. Experimental evidences of redistribution phenomenon in supercapacitors and consequent improvement of their dynamic model IEEE Grenoble Conference. Grenoble, France: IEEE 2013; 2013:1–7. https://doi.org/10.1109/PTC.2013.6652413.
[29] Pell WG, Conway BE, Adams WA, de Oliveira J. Electrochemical efficiency in multiple dischargerrecharge cycling of supercapacitors in hybrid EV applications 1999.
[30] Torregrossa D, Bahramipanah M, Namor E, Cherkaoui R, Paolone M. Improvement of dynamic modeling of supercapacitor by residual charge effect estimation. IEEE Trans Ind Electron 2014;61:1345–54. https://doi.org/10.1109/TIE.2013.2259780.
[31] Cheon SJ, Hong SG, Lee JH, Nam YS. Design and performance analysis of a 500-W heat source for radioisotope thermophotovoltaic converters. Int J Energy Res 2018;42:817–29. https://doi.org/10.1002/er.3889.